Electronic Supplementary Information

Dynamic metallopolymer networks: A protocol to quantify Pt(II)···Pt(II) and π−π stacking interactions

Xiandeng Qiu,[a#] Xiao Cao,[c#] Huanting Huang,[a] Qun He,[a] Guanjun Chang,[d] Quan Chen*[c] and Weifeng Bu*[ab]

[a] Key Laboratory of Nonferrous Metals Chemistry and Resources Utilization of Gansu Province, State Key Laboratory of Applied Organic Chemistry, and College of Chemistry and Chemical Engineering, Lanzhou University, Lanzhou, 730000, China. E-mail: buwf@lzu.edu.cn

[b] State Key Laboratory of Solid Lubrication, Lanzhou Institute of Chemical Physics, Chinese Academy of Sciences, Lanzhou, 730000, China

[c] State Key Laboratory of Polymer Physics and Chemistry, Changchun Institute of Applied Chemistry, Chinese Academy of Sciences, Changchun 130022, China. E-mail: qchen@ciac.ac.cn

[d] State Key Laboratory of Environment-friendly Energy Materials & School of Material Science and Engineering, Southwest University of Science and Technology, Mianyang, 621010, China

[#]X. Qiu and X. Cao contributed equally to this work.

Experimental Section

Materials and Instruments.

$[Pt(Me_2bzimpy)Cl]^+Cl^-$ ($Me_2bzimpy$ = 2,6-bis(*N*-methylbenzimidazol-2′-yl) pyridine),[S1−S6] $[Pt(MeOMe_2bzimpy)Cl]^+Cl^-$ ($MeOMe_2bzimpy$ = 4-methoxy-2,6-bis(*N*-methylbenzimidazol-2′-yl)pyridine,[S1−S6] **TPS-L-I** (M_n = 13.6 kg/mol, $Đ$ = 1.07),[S7] **TPS-L-II** (M_n = 12.6 kg/mol, $Đ$ = 1.07),[S7] and randomly sodium sulfonated polystyrene (**SPS-Na**, M_w = 13.5 kg/mol, $Đ$ = 1.06)[S8] were synthesized as described in the previous literatures. One molecular **SPS-Na** contained ca. 2.0 sodium-styrenesulfonate units. Other commercially available solvents and chemicals were directly used without any further purification.

^{1}H NMR spectra were recorded on a JNM-ESC400 spectrometer, during which the samples were dissolved in C*D*Cl$_3$ and tetramethylsilane was used as an internal standard. Size-exclusion chromatography (SEC) plots were recorded on a Waters 1515 instrument, leading to number-average molecular weight (M_n), weight-average molecular weight (M_w), and molar mass dispersity ($Đ$) of difunctional polystyrenes. Polystyrene was used as a calibration standard, and tetrahydrofuran (THF) was the eluent at a flow rate of 1.0 mL/min. The column temperature was kept at 40 °C. Fourier transformation infrared spectra (FT-IR, KBr) were performed with a Nicolet NEXUS 670 spectrometer. The thermal measurements were carried out using a TA Q20 differential scanning calorimeter (DSC) with nitrogen gas purging at a flow rate of 50 mL/min. All DSC experiments were conducted at a heating/cooling rate of 10 °C/min in a range from 0 °C to 190 °C. Two heating−cooling runs were conducted and the glass-transition temperature T_g was determined from the second runs, with the aid of the commercially available Universal Analysis software.

Small angle X-ray scattering (SAXS) experiments were performed using NanoSTAR-U (BRUKER AXS INC.) with Cu K$_\alpha$ radiation (λ = 0.154 nm) at room temperature and 140 °C. The generator was operated at 40 kV and 650 μA. The sample-to-detector distance was chosen to be LSD = 1122 mm, and two-dimensional SAXS

patterns were obtained using a HI-STAR detector. All data were corrected in a range of effective scattering vector $q = (4\pi\sin\theta)/\lambda$ from 0.08 to 2.0 nm^{-1}, with 2θ being the scattering angle at room temperature, and the background scattering was corrected. Wide-angle X-ray scattering (WAXS) measurements were carried out using a Rigaku SmartLab diffractometer with Cu K_α radiation ($K_{\alpha1}$ line, with $\lambda = 0.154$ nm). The X-ray source was operated at 40 kV and 40 mA. The WAXS patterns of the samples were obtained at a step scan rate of 0.03° per 3 s in a scattering angle (2θ) range of 0.5−30°, corresponding to a scattering vector q of 0.35−21.11 nm^{-1}, with θ being a half of the scattering angle. The WAXS measurements performed at 140 °C were under a reflection mode, while others were under transmission modes.

All rheological measurements were conducted with a strain-controlled rheometer (ARES-G2, TA) using 8 mm parallel-plate fixtures. The measurements were under the protection of dry N_2. The frequency sweep measurements were conducted within an angular frequency range of 0.1−100 rad/s in the temperature range of 120 to 190 °C, and the stress relaxation measurements were conducted at 190 °C to shorten the time of measurement at high T. For both the frequency sweep and stress relaxation measurements, the strain amplitude was kept in the linear regime, as verified from the strain amplitude sweeps. The stress relaxation modulus, a function of time t, is transferred into the storage and loss moduli as functions of angular frequency.

Synthetic Procedures and Characterization Details.

TPS-Pt-I: TPS-L-I[S7] (1 g, 0.071 mmol) and K_2PtCl_4 (88 mg, 2.12 mmol) were added to DMSO/$CHCl_3$ (10 mL/30 mL) in an oven dried Schlenk flask under an argon atmosphere. The resulting mixture solution was placed in a thermostatic oil bath held at 90 °C and stirred for 4 d. After the completion of the reaction, the obtained orange solution was cooled to room temperature, and the solvent was distilled off under reduced pressure. The obtained crude product was dissolved in dichloromethane (20 mL), NH_4PF_6 (665 mg, 4.08 mmol) was added dropwise, and the solution was continuously stirred at room temperature for 2 days. The orange solution was cooled to room temperature and the solvents were removed by distilling under vacuum conditions.

An orange red solid was collected by filtration and further washed with cold methanol (100 mL). The yield was 95% (0.99 g) based on the **TPS-L-I** ligand. Anal. Calcd. for **TPS-Pt-I**, $C_{1050}H_{1062}Cl_2F_{12}N_{16}O_6P_2Pt_2$: C, 85.48; H, 7.26; N, 1.52. Found: C, 85.44; H, 7.28; N, 1.54.

TPS-Pt-II: TPS-Pt-II was synthesized according to the similar procedure for **TPS-Pt-I**, but using **TPS-L-II**[S7] as a polymer ligand. Yield: 1.01 g, 97%. Anal. Calcd. for **TPS-Pt-II**, $C_{1052}H_{1066}Cl_2F_{12}N_{16}O_8P_2Pt_2$: C, 85.30; H, 7.25; N, 1.51. Found: C, 85.48; H, 7.23; N, 1.48.

SPS-Pt-I: $[Pt(Me_2bzimpy)Cl]^+Cl^-$ (53.3 mg, 0.088 mmol) was dissolved in 20 mL of water. The resulting solution was treated with solid powders of **SPS-Na**[S8] (300 mg, 0.044 mmol, based on the unit of sodium styrenesulfonate) with vigorous stirring for 3 days. Such a long reaction allowed a full ionic exchange of **SPS-Na** with $[Pt(Me_2bzimpy)Cl]^+Cl^-$.[S9] The orange red solid was collected by filtration, washed with methanol, and dried in *vacuum*. The yield was 96% (311 mg) based on the **SPS-Na**. Anal. Calcd. for **SPS-Pt-I**, $C_{1018}H_{1008}Cl_2N_{10}O_6Pt_2S_2$: C, 87.31; H, 7.26; N, 1.00; S, 0.46. Found: C, 87.07; H, 7.23; N, 0.94; S, 0.30.

SPS-Pt-II: SPS-Pt-II was synthesized according to the similar procedure for **SPS-Pt-I**, but using $[Pt(MeOMe_2bzimpy)Cl]^+Cl^-$ as a reactant. Yield: 312 mg, 95%. Anal. Calcd. for **SPS-Pt-II**, $C_{1020}H_{1012}Cl_2N_{10}O_8Pt_2S_2$: C, 87.11; H, 7.25; N, 1.00; S, 0.46. Found: C, 82.87; H, 7.34; N, 1.33; S, 0.27.

Additional results and discussion.

Synthesis and Characterization. The $[Pt(Me_2bzimpy)Cl]^+PF_6^-$-containing telechelic polymers of **TPS-Pt-I** and **TPS-Pt-II** were synthesized by reacting K_2PtCl_4 with **TPS-L-I** and **TPS-L-II** and subsequent metathesis with NH_4PF_6, respectively (Fig. S1). Such coordination reactions were quantitative, consistent with our previously reported result.[S10-S13] For both **TPS-Pt-I** and **TPS-Pt-II**, the characteristic FT-IR absorptions of PF_6^- appeared at 843 and 555 cm^{-1} (Fig. S2).[S11–S13] In the resulting ^1H NMR spectra, the proton signals of bzimpy groups disappeared completely, while the proton signals of polystyrenes remained (Fig. S3 and S4). This was due to the

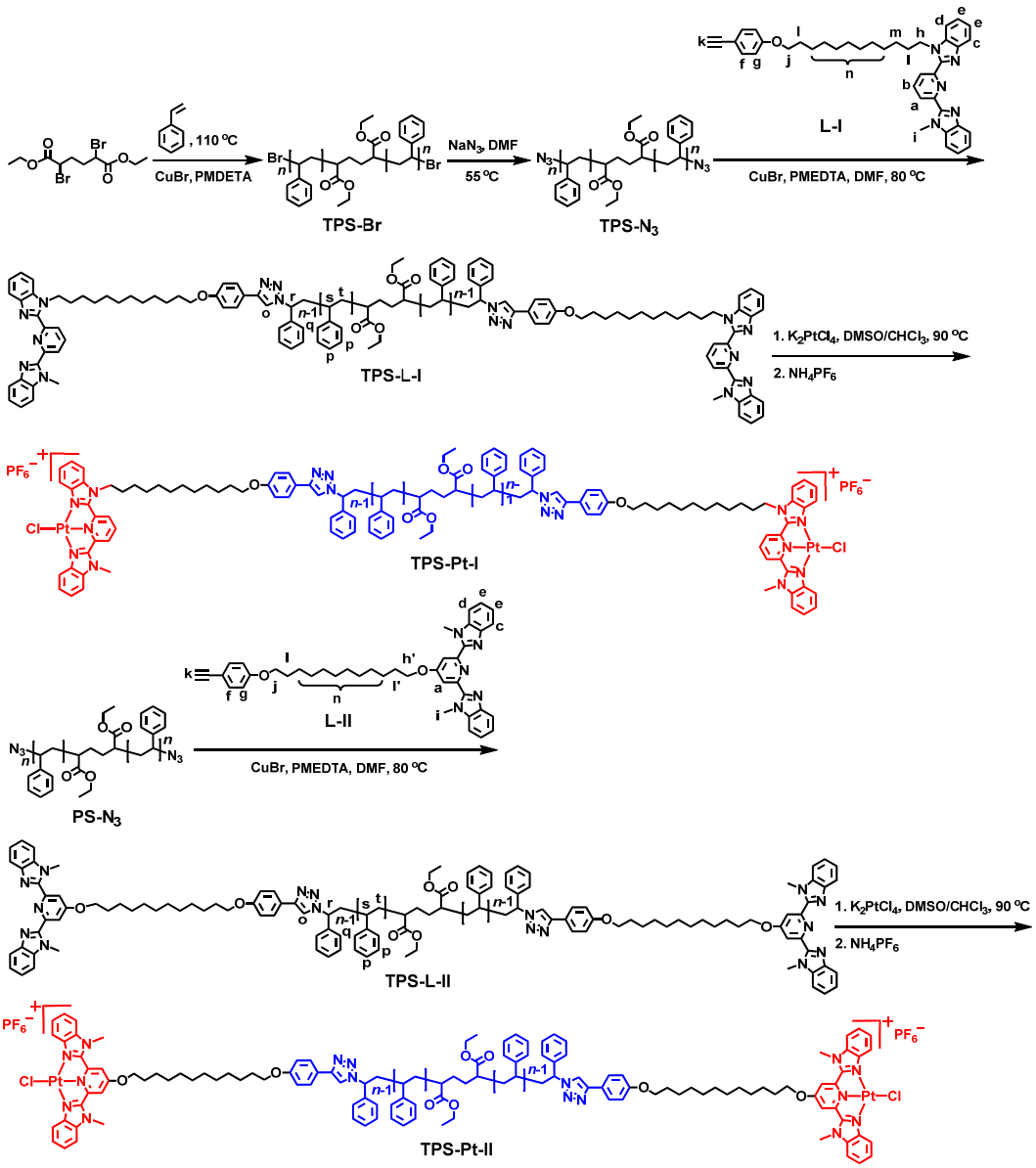

Fig. S1. Synthetic routes of $[Pt(bzimpy)Cl]^{+}PF_6^{-}$-containing telechelic polymers.[S7]

formation of aggregates stemming from Pt(II)···Pt(II) and/or π–π stacking interactions of the planar platinum(II) blocks at a high concentration (30 mg/mL in C*D*Cl$_3$).

^{1}H NMR spectra discussion. The coordination reactions between small-molecule bzimpy and K_2PtCl_4 were quantitative in dimethyl sulfoxide (DMSO) or DMSO-based mixture solvents.[S1,S14] The resulting $[Pt(bzimpy)Cl]^{+}$ complexes have been well characterized by ^{1}H NMR spectra, in which the proton signals of bzimpy showed clear downfield or upfield shifts after the coordinating reactions.

In the case of ABC triblock metallopolymers that contain octadecyl and PEG chains and $[Pt(bzimpy)Cl]^+$ complexes, sequentially, the downfield or upfield shifts of bzimpy were also observed clearly after the coordinating reactions.[S10]

However, in the cases of polystyrene-$[Pt(bzimpy)Cl]^+$ metallopolymers, the proton resonances of bzimpy groups disappeared completely in the ^{1}H NMR spectra, while the proton signals of polystyrenes remained. This was presumably due to the formation of aggregates stemming from Pt···Pt and/or π–π stacking interactions of the planar platinum(II) blocks at a high concentration (30 mg/mL).[S7,S12,S13]

UV-vis absorption and luminescence spectra. Here, the $[Pt(bzimpy)Cl]^+$ complexes were categorized into two types: platinum(II) 2,6-bis(alkylbenzimidazol-2′-yl)pyridine complexes (**Pt-I**) and platinum(II) 2,6-bis(alkylbenzimidazol-2′-yl)-4-alkyloxypyridine complexes (**Pt-II**), where the alkyl groups can be methyl, dodecyl, and/or other.

Generally, the solution UV-vis absorption spectra of $[Pt(bzimpy)Cl]^+$-functionalized polymers showed intense, structured absorption bands at 310−390 nm and moderately intense bands at 410−500 nm.[S7,S10−S13,S15] With reference to the previous spectroscopic studies on $[Pt(bzimpy)Cl]^+$-derived complexes (**Pt-I** and **Pt-II**),[S1,S14] the former was assigned as an intraligand (π→π*) transition of the bzimpy ligands, while the latter was attributed to a metal-to-ligand charge-transfer transition (MLCT, dπ(Pt)→π*(bzimpy)).

With increasing the concentrations of **Pt-I**-containing polymers (10^{-6} to 10^{-4} mol/L for), lower-energy absorption shoulders at ca. 550 nm became increasingly recognizable, which were assignable as metal–metal-to-ligand charge-transfer (MMLCT, dσ*(Pt_2)→π*(bzimpy)) transitions that arose from intermolecular and/or intramolecular Pt(II)···Pt(II) and π–π stacking interactions between the planar platinum(II) units.[S7,S10−S13] However, no such shoulders were observed in the series of **Pt-II**-containing polymers, indicating that only π–π stacking interactions occurred between the **Pt-II** units.[S10,S15]

Therefore, in our opinion, the aforementioned spectroscopic assignments for the

[Pt(bzimpy)Cl]$^+$ complexes and their corresponding metallopolymers have also been well accepted.[S1,S7,S10−S15]

As addressed, the vibronic-structured, monomeric emissions of [Pt(bzimpy)Cl]$^+$ complexes (single Pt units) appeared at 540 and 580 nm for **Pt-I** and 560 and 600 nm for **Pt-II**, respectively.[S12,S13] In the present study, structureless emission bands appeared at λ_{max} = 666, 626, 650, and 628 nm for **TPS-Pt-I**, **TPS-Pt-II**, **SPS-Pt-I**, and **SPS-Pt-II**, respectively (Fig. 2b), which were signficantly red-shifted compared with the monomeric emissions. Therefore, one of biexponential emission decays cannot be single Pt units.

SAXS/WAXS results of TPS-Pt-I, TPS-Pt-II, SPS-Pt-I, and SPS-Pt-II at 140 °C. We have performed the SAXW/WAXS measurements of **TPS-Pt-I**, **TPS-Pt-II**, **SPS-Pt-I**, and **SPS-Pt-II** at 140 °C (Fig. S8). The resulting SAXW/WAXS plots of **TPS-Pt-I** and **SPS-Pt-I** were comparable with those at room temperature, indicative of similar organized micellar constructs, respectively. In the case of **TPS-Pt-II**, much more organized micelles were observed at 140 °C than at room temperature, while for **SPS-Pt-II**, much sharper WAXS signals of the [Pt(Me$_3$bzimpy)Cl]$^+$ complexes appeared at (6.44 nm^{-1} and 0.98 nm) and (7.05 nm^{-1} and 0.89 nm). Both of them were presumably due to the melt-induced organizations of **TPS-Pt-II** and **SPS-Pt-II** at 140 °C. Moreover, the WAXS signals of the metallopolymers were observed clearly at (18.6 nm^{-1} and 3.38 Å). This, together with the above spectroscopic assignments, confirmed the presence of Pt(II)···Pt(II) and π–π stacking interactions in **TPS-Pt-I** and **SPS-Pt-I**, and π–π stacking interactions in **TPS-Pt-II** and **SPS-Pt-II** at 140 °C. These organization trends agreed well with those occurring at room temperature.

Rheological discussion. In the present study, the choice of the samples are quite representative, as addressed in the TEXT. Based on the position of the stickers, the ionomers are generally classified as random ionomers and telechelic ionomers. The fixed ion-ion distance in the telechelic ionomers usually leads to larger assembled structure, which has been demonstrated in the current system. For either random or telechelic ionomers, once the ion-ion distance along the backbone is much larger than

the Kuhn length, the dissociation events (of different stickers) are relatively independent, and then the association energy does not rely on the ion content once the species of the ionic group and polymer backbone have been fixed.[S16] In the opposite case, if the ion-ion distance is smaller than the Kuhn length, the neighboring ionic groups are forced to exhibit coupling motion and then the association energy increase significantly.

This argument has been justified in the series of study by Chen et al.[S16] For example, the evolution of linear viscoelasticity of sulfonated PS with sodium as counterion (SPS-Na), either unentangled or entangled, can be consistently predicted using the reversible gelation model with A SINGLE ASSOCITION ENERGY.

Table S1. Molecular Characteristics of TPS-L-I, TPS-L-II, TPS-Pt-I, TPS-Pt-II, SPS-Na, SPS-Pt-I, and SPS-Pt-II

Sample	M_n [a] (kg/mol)	$Đ$ [a]	$M_{n,NMR}$ [b] (kg/ mol)	Sample	M_n (kg/ mol)
TPS-L-I	13.6	1.07	14000	**TPS-Pt-I**	14.7 [c]
TPS-L-II	12.6	1.07	14100	**TPS-Pt-II**	14.8 [c]
SPS-Na	12.7	1.06	-	**SPS-Pt-I**	13.8 [d]
SPS-Na	12.7	1.06	-	**SPS-Pt-II**	13.9 [f]

[a] The values of M_n, M_w, and M_w/M_n ($Đ$) were determined by SEC. The data of **TPS-L-I/II**[S7] and **SPS-Na**[S8] were reported previously. [b] The values of $M_{n,NMR}$ were calculated by ^{1}H NMR spectroscopy. [c] The M_n values of platinum(II)-containing telechelic metallopolymers (**TPS-Pt-I** and **TPS-Pt-II**) were obtained by adding the molecular weight of $Pt_2Cl_2P_2F_{12}$ with the corresponding polymer ligands. The M_n values of **SPS-Pt-I** [d] and **SPS-Pt-II** [f] were obtained by adding the molecular weights of $C_{42}H_{34}Cl_2N_{10}Pt_2$ and $C_{44}H_{38}Cl_2N_{10}O_2Pt_2$ with the randomly sulfonated polystyrene, respectively.

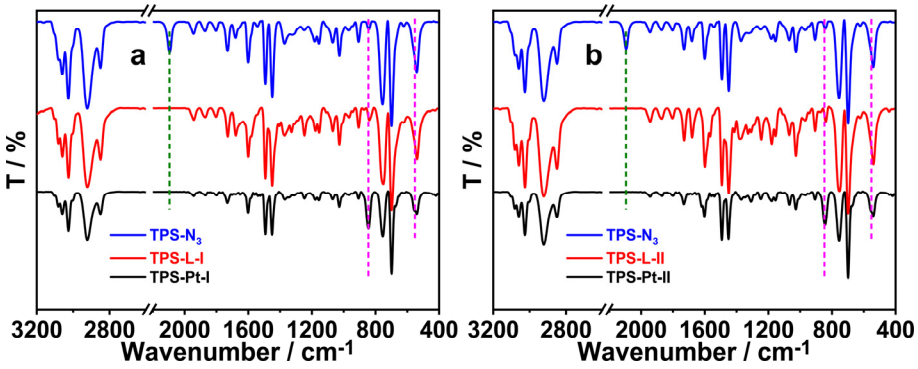

Fig. S2. FT-IR spectra of **TPS-N$_3$**,[S7] **TPS-L-I**,[S7] and **TPS-Pt-I** (a) and **TPS-N$_3$**,[S7] **TPS-L-II**,[S7] and **TPS-Pt-II** (b).

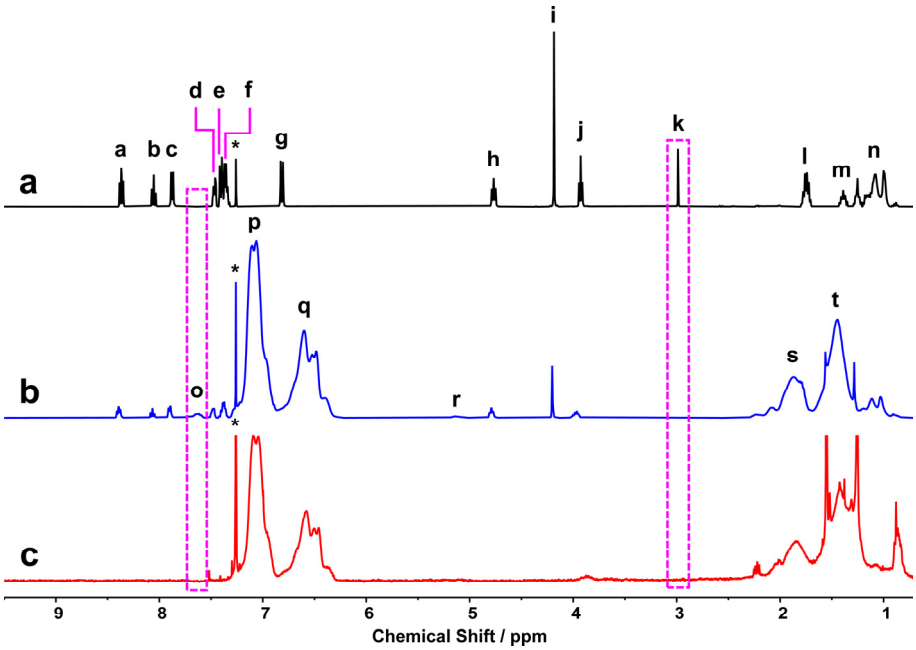

Fig. S3. ^{1}H NMR spectrum of **L-I** (a),[S7] **TPS-L-I** (b)[S7] and **TPS-Pt-I** (c). The * signals referred to the residual $CHCl_3$ in $CDCl_3$. The proton signals were identified in the chemical structures of **L-I**[S7] and **TPS-L-I**[S7] as shown in Fig. S1.

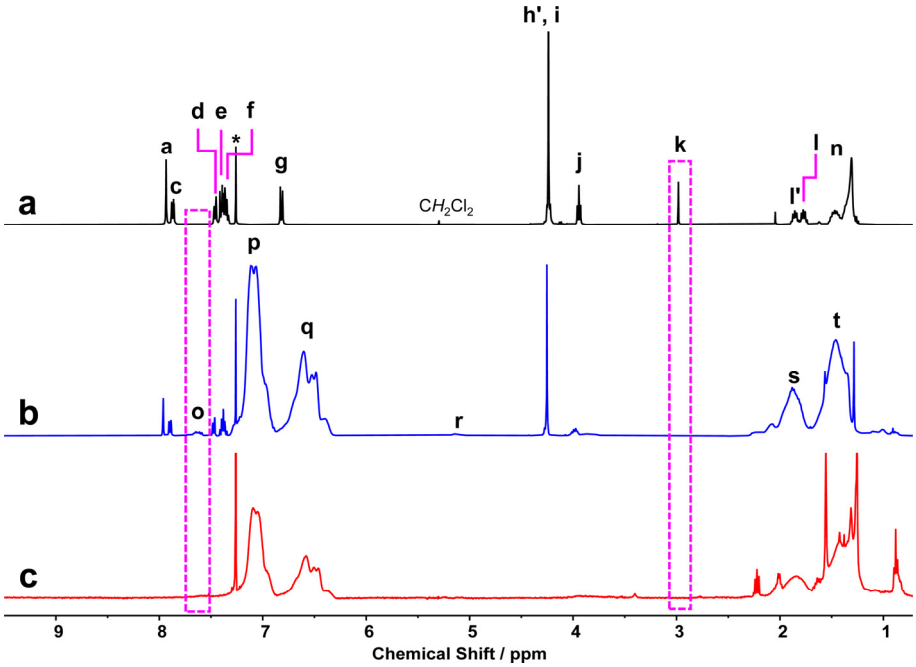

Fig. S4. ^{1}H NMR spectrum of **L-II** (a),[S7] **TPS-L-II** (b)[S7] and **TPS-Pt-II** (c). The * signals referred to the residual $CHCl_3$ in $CDCl_3$. The proton signals were identified in the chemical structures of **L-II**[S7] and **TPS-L-II**[S7] as shown in Fig. S1.

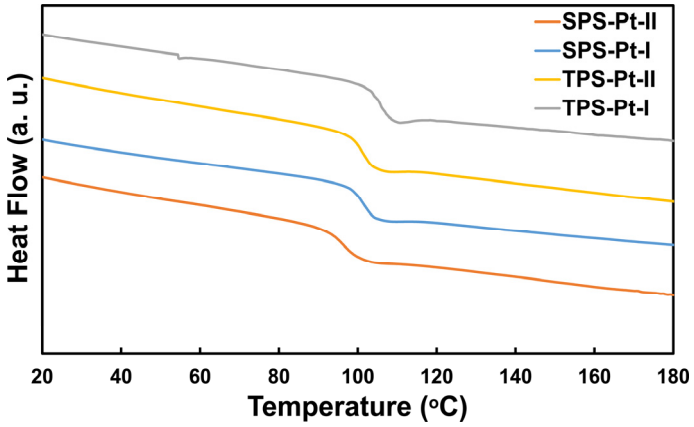

Fig. S5. DSC traces of **TPS-Pt-I**, **TPS-Pt-II**, **SPS-Pt-I**, and **SPS-Pt-II**.

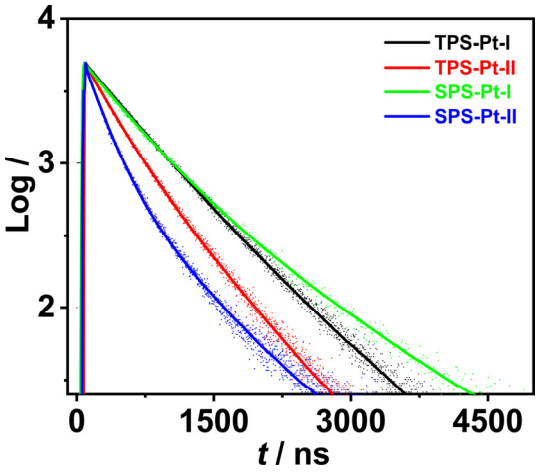

Fig. S6. The luminescence decay profiles of **TPS-Pt-I**, **TPS-Pt-II**, **SPS-Pt-I**, and **SPS-Pt-II** were well-fitted by double-exponential curves. The fitting results were summarized in **Table S2**.

Table S2. The Luminescence Lifetimes and Quantum Yields of TPS-Pt-I, TPS-Pt-II, SPS-Pt-I, and SPS-Pt-II

sample	MMLCT λ_{abs} / nm	λ_{em} / nm	Φ / %	τ_1 / ns [a]	τ_2 / ns [a]
TPS-Pt-I	552	665	49.8	513.41	846.58
TPS-Pt-II	- [b]	626	12.5	306.99	618.45
SPS-Pt-I	550	650	33.8	460.41	984.57
SPS-Pt-II	- [b]	628	6.70	205.52	609.18

[a] Relative weighting (RW) of components in double exponential fits. [b] No MMLCT absorption shoulder bands were detected in the UV−vis diffuse reflectance spectra of **TPS-Pt-II** and **SPS-Pt-II**.

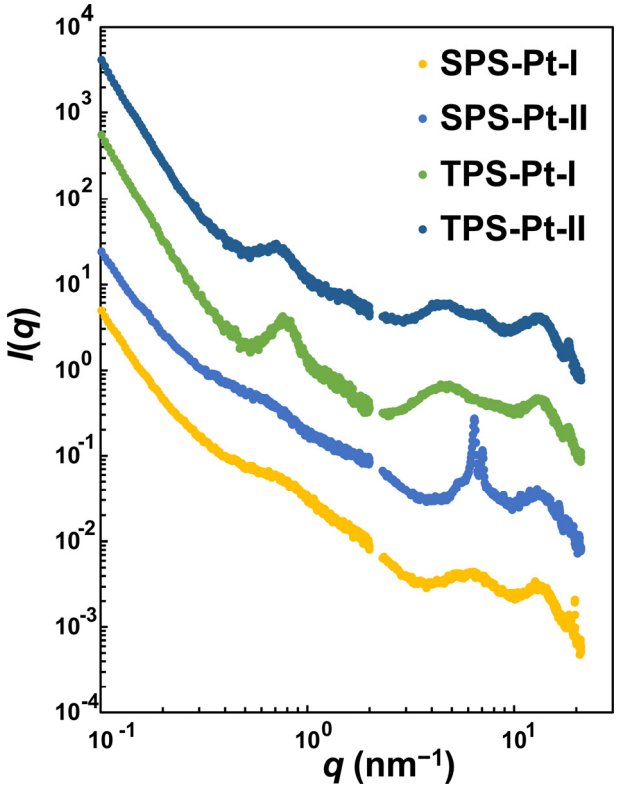

Fig. S7 SAXS and WAXS plots of **TPS-Pt-I**, **TPS-Pt-II**, **SPS-Pt-I**, and **SPS-Pt-II** at 140 °C.

X-ray scattering Fitting. The scattering profiles of **TPS-Pt-I**, **TPS-Pt-II**, and **SPS-Pt-I** are compared in Fig. 3 in text, and each profile shows three peaks at high q > 2 nm^{-1}, where the low, medium, and high q peaks reflect the spacing correlation between the ionic clusters filled with the [Pt(bzimpy)Cl]$^+$ complexes, the backbones and amorphous side chains of polystyrene blocks, respectively. The main peak and shoulder peak at low q < 2 nm^{-1} reflect networked flowerlike micelles. Three Lorentzian functions are used to fit three peaks at q > 2 nm^{-1}, and the Percus-Yevick model[S17] and a power law term are used to fit the scattering profile at q < 2 nm^{-1},

$$I(q) = L_a(q) + L_b(q) + L_c(q) + I_{ion}(q) + Bq^{-2} \quad \text{(S1)}$$

where LX(q) = $MK^2/[(q-q_X)^2 + K^2]$, with X = a, b, and c representing the side chain, backbone, and ionic cluster correlations, respectivly, and the Bq^{-2} term representing the upturn at the lowest q. Three parameters are adjusted in the fitting, i.e., the peak position, qX, the half-width at half-maximum, K, and an intensity factor, M.

The Percus-Yevick Module works well for the micellar structure and the scattering

intensity is given by a sum of a product of a structure factor and a form factor and a flat background.

$$I(q) = KS(qR_2)\int_{R_1=0}^{\infty} \Phi(qR_1)\, f_p(R_1, \overline{R_1}, \sigma) dR_1 + C \quad \text{(S2)}$$

Here K is a contrast factor depending on the electron density difference between the particles and the matrix, C is the scattering background measured at large q vectors. The structure factor of a system of the hard sphere is given by $S(qR_2)$. It depends on the scattering vector q and the radius R_2 of the hard spheres. The latter corresponds in our case to the outer radius of the micelles. $S(qR_2)$ is given by

$$S(qR_2) = (1 + \frac{24fG(x)}{x})^{-1} \quad \text{(S3)}$$

where $x = 2qR_2$, and f is the volume fraction of the hard.

$$G(x) = \frac{\alpha}{x^2}(sinx - xcosx)$$

$$+\frac{\beta}{x^3}(2xsinx + (2 - x^2)cosx - 2)$$

$$+\frac{\gamma}{x^5}(-x^4 cosx + 4[(3x^2 - 6)cosx + (x^3 - 6x)sinx + 6]) \quad \text{(S4)}$$

Here, α, β and γ are functions of the volume fraction f.

$$\alpha = \frac{(1+2f)^2}{(1-f)^4}\ ,\ \beta = \frac{-6f(1+f/2)^2}{(1-f)^4}\ ,\ \gamma = \frac{1/2f(1+f/2)^2}{(1-f)^4} \quad \text{(S5)}$$

(q) is the form factor of the scatter objects. In the present case, the scattering arises from the core of spherical micelles with radius R_1 is,

$$\Phi(qR_1) = [\mu \frac{3}{(qR_1)^3}[\sin(qR_1) - qR_1 \cos(qR_1)]]^2 \quad \text{(S6)}$$

where μ is the volume of the core. In a real system, the size of the core shows a distribution, and thus we include a probability distribution $f_p(R_1, \overline{R_1}, \sigma)$ for R_1, where $\overline{R_1}$ and σ are the mean value for the radius and the width of the distribution, respectively. A consistent description of the data can be achieved using a lognormal distribution of R_1,

$$f_p(R_1, \overline{R_1}, \sigma) = \frac{1}{R_1\sigma\sqrt{2\pi}} e^{-\frac{(\ln R_1 - \ln \overline{R_1})^2}{2\sigma^2}} \quad \text{(S7)}$$

The parameter (f, $\overline{R_1}$, R_2, σ, C) were determined from a fit to the data. All important parameters of the fitting based on eqs S1-S7 are summarized in Table S4.

Table S3 Fitting Parameters Determined from Fitting the X-Ray Scattering Results at 25 °C

	Parameters	**SPS-Pt-I**	**TPS-Pt-I**	**TPS-Pt-II**
L_a	M	0.022	0.0057	0.0077
	K	2.5	3.4	3.2
	q_a	13.4	13.3	13.7
L_b	M	0.0075	0.0026	0.005
	K	2	1.8	3
	q_b	7.3	8	7
L_c	M	0.019	0.0093	0.009
	K	1.8	1.6	1.8
	q_c	4.4	4.1	3.2
I_{PY}	R_1	0.68	1.07	0.65
	R_2	4.2	4.0	3.8
	f	0.1482	0.352	0.0439
	σ	0.51	0.4	0.83
	K	0.00054	0.00004	0.000055
	C	0.013	0.0008	0

Table S4. The Rouse Time per Kuhn Segment, τ_0, Sticker Lifetime, τ_s, and Association Energy for Sticker Dissociation, E_a

Samples	SPS-Na [a]	SPS-K [a]	TPS-Rb [a]	TPS-Cs [a]	**SPS-Pt-I**	**TPS-Pt-I**	**SPS-Pt-II**		**TPS-Pt-II**
T_g (°C)	102	102	102	102	102	105	96		102
τ_0 (μs)	32	32	32	32	32	32	32	32	32
τ_s (s)	4500	770	160	47	175	199520	10	33110	- [b]
E_a (kJ/mol)	65	58	53	49	53	77	44	71	- [b]

[a] The data were reported previously.[S18] [b] The τ_s of π–π stacking interactions of **TPS-Pt-II** were out of the present LVE observation.

REFERENCES

(S1) L. J. Grove, J. M. Rennekamp, H. Jude and W. B. Connick, *J. Am. Chem. Soc.*, 2004, **126**, 1594.

(S2) N. Liu, B. Wang, W. Liu and W. Bu, *Chem. Commun*., 2011, **47**, 9336.

(S3) N. Liu, B. Wang, W. Liu and W. Bu, *J. Mater. Chem. C*, 2013, **1**, 1130.

(S4) N. Liu, Q. He and W. Bu, *Langmuir*, 2015, **31**, 2262.

(S5) N. Liu, Q. He, Y. Wang and W. Bu, *Soft Matter*, 2017, **13**, 4791.

(S6) L. Hu, F. Qu, Y. Wang, J. Shen, Q. He, B. Zhang and W. Bu, *J. Mater. Chem. C*, 2017, **5**, 12500.

(S7) X. Qiu, H. Xue, L. Xu, R. Wang, S. Qiu, Q. He and W. Bu, *Polym. Chem.*, 2021, **12**, 5191.

(S8) C. Huang, C. Wang, Q. Chen, R. H. Colby and R. A. Weiss, *Macromolecules*, 2016, **49**, 3936.

(S9) Y. Liao, N. Liu, Q. Zhang and W. Bu, *Macromolecules*, 2014, **47**, 7158.

(S10) W. Meng, X. Qiu, R. Wang, Q. He and W. Bu, *J. Mater. Chem. C*, 2020, **8**, 15616.

(S11) W. Meng, Q. He, M. Yu, Y. Zhou, C. Wang, B. Yu, B. Zhang and W. Bu, *Polym. Chem.*, 2019, **10**, 4477.

(S12) N. Liu, Y. Wang, C. Wang, Q. He and W. Bu, *Macromolecules*, 2017, **50**, 2825.

(S13) F. Qu, B. Yang, Q. He and W. Bu, *Polym. Chem.*, 2017, **8**, 4716.

(S14) (*a*) E. J. Rivera, C. Figueroa, J. L. Colón, L. Grove and W. B. Connick, *Inorg. Chem.* 2007, **46**, 8569; (*b*) K. Wang, M. A. Haga, H. Monjushiro, M. Akiba amd Y. Sasaki, *Inorg. Chem.*, 2000, **39**, 4022; (*c*) A. Y. Y. Tam, W. H. Lam, K. M. C. Wong, N. Zhu and V. W.-W. Yam, *Chem. Eur. J.*, 2008, **14**, 4562; (*d*) I. Mathew and W. Sun, *Dalton Trans.*, 2010, **39**, 5885; (*e*) C. Po, A. Y.-Y. Tam, K. M.-C. Wong and V. W.-W. Yam, *J. Am. Chem. Soc.*, 2011, **133**, 12136; (*f*) N. Liu, B. Wang, W. Liu and W. Bu, *J. Mater. Chem. C,* 2013, **1**, 1130; (*g*) J. Liang, X. Zheng, L. He, H. Huang and W. Bu, *Dalton Trans.,* 2014, **43**, 13174; (*h*) J. Liang, H. Huang, L. He, N. Liu, Y. Chen and W. Bu, *Dalton Trans.,* 2015, **44**, 66.

(S15) Q. He, C. Wang, J. Xiao, Y. Wang, Y. Zhou, N. Zheng and W. Bu, *J. Mater.*

Chem. C, 2018, **6**, 12187.

(S16) (*a*) Q. Chen, C. Huang, R. A. Weiss and R. H. Colby, *Macromolecules*, 2015, **48**, 1221; (*b*) C. Huang, C. Wang, Q. Chen, R. H. Colby and R. A. Weiss, *Macromolecules*, 2016, **49**, 3936; (*c*) X. Cao, X. Yu, J. Qin and Q. Chen, *Macromolecules*, 2019, **52**, 8771.

(S17) (*a*) T. Yan, K. Schröter, F. Herbst, W. H. Binder and T. Thurn-Albrecht, *Macromolecules*, 2014, **47**, 2122; (*b*) T. Yan, K. Schröter, F. Herbst, W. H. Binder and T. Thurn-Albrecht, *Macromolecules*, 2017, **50**, 2973.

(S18) S. Liu, X. Cao, C. Huang, R. A. Weiss, Z. Zhang and Q. Chen, *ACS Macro Lett.*, 2021, **10**, 503.